Journal of Alloys and Compounds 509 (2011) 6893–6898

Contents lists available at ScienceDirect

Journal of Alloys and Compounds

journal homepage: www.elsevier.com/locate/jallcom

Synthesis of core–shell Fe_3O_4@SiO_2@MS (M = Pb, Zn, and Hg) microspheres and their application as photocatalysts

Zhenghua Wang*, Shiyu Zhu, Suping Zhao, Haibo Hu

Anhui Key Laboratory of Functional Molecular Solids, College of Chemistry and Materials Science, Anhui Normal University, Wuhu 241000, PR China

ARTICLE INFO

Article history:
Received 20 December 2010
Received in revised form 25 March 2011
Accepted 30 March 2011
Available online 6 April 2011

Keywords:
Composite materials
Core–shell structure
Photocatalysis

ABSTRACT

In this work, we report the fabrication of core–shell Fe_3O_4@SiO_2@MS (M = Pb, Zn, and Hg) microspheres through a wet-chemical approach. The Fe_3O_4@SiO_2@MS microspheres have both ferromagnetic and photocatalytic properties. The sulfide nanoparticles on the surfaces of microspheres can degrade organic dyes under the illumination of UV light. Furthermore, the microspheres are easily separated from the solution after the photocatalytic process due to the ferromagnetic Fe_3O_4 core. The photocatalysts can be recycled for further use with slightly lower photocatalytic efficiency.

1. Introduction

In recent years, core–shell multi-components have attracted intense attention because of their potential applications in electronics, magnetism, optics, and catalysis [1–5]. Different from single-component that can only supply people with one function, the core–shell multi-components can integrate multiple functions into one system for specific applications [6–10]. Moreover, the interactions between different components can greatly improve the performance of the multi-components system and even generate new synergetic properties.

Among the core–shell structured composites, the composites with magnetic core and functional shell structures have received especial attention because of their potential applications in catalysis, drug storage/release, selective separation, chromatography, and chemical or biologic sensors [11–16]. The magnetic core has good magnetic responsibility, and can be easily magnetized. Therefore, the composites with magnetic core can be conveniently collected, separated or fixed by external magnet. The functional shell such as semiconductors, SiO_2 and metals can be applied for specific applications. For example, the Fe_3O_4@silica and Fe_3O_4@Chitosan core–shell microspheres can be applied as adsorbents to remove heavy metal ions from wastewater [17,18], the Fe_3O_4@TiO_2 core–shell microspheres can be used for selective enrichment of phosphopeptides in phosphoproteome analysis [19], and the Ag-coated Fe_3O_4@SiO_2 microspheres can be served as surface-enhanced Raman spectroscopy (SERS) substrates [20].

Herein, core–shell microspheres of Fe_3O_4@SiO_2@MS (M = Pb, Zn, and Hg) were synthesized by a wet-chemical approach involves several steps. Firstly, a layer of SiO_2 was coated on Fe_3O_4 microspheres, and then, sulfide nanoparticles were coated onto the SiO_2 layer. The SiO_2 layer is flexible and adhesive, which makes the core–shell structure more stable. Moreover, the density of sulfide nanoparticles on the core–shell microspheres can be controlled by tuning the amount of metal ions adsorbed by the SiO_2 layer. The prepared Fe_3O_4@SiO_2@MS microspheres are multi-functional. The Fe_3O_4 core makes them very easy to be separated and recycled from solution with the help of an external magnet, and the semiconductor sulfides can act as photocatalysts to decompose organic dyes in wastewater.

2. Experimental

All reagents were commercial available from Sinopharm Chemical Regent Co., Ltd. with analytical grade and were used without further purification.

2.1. Synthesis of Fe_3O_4 microspheres

The synthesis was carried out through a hydrothermal process according to a previous report [21]. Typically, 1.35 g of iron chloride (III) hexahydrate was dissolved in 40 mL ethylene glycol to form a clear solution, then 1.0 g of polyethylene glycol (Mw = 4000) and 3.6 g of sodium acetate trihydrate was added subsequently. The mixture was stirred until the reactants were fully dissolved. After that, the mixture was transferred into a Teflon lined autoclave with a capacity of 50 mL and heated at 200 °C for 8 h. The products were collected and fully rinsed with deionized water and absolute ethanol with the help of an external magnet. Finally, the products were dried under vacuum at 60 °C for 2 h for further use.

* Corresponding author. Tel.: +86 553 3869303; fax: +86 553 3869302.
E-mail address: zhwang@mail.ahnu.edu.cn (Z. Wang).

0925-8388/$ – see front matter © 2011 Elsevier B.V. All rights reserved.
doi:10.1016/j.jallcom.2011.03.175

2.2. Synthesis of Fe_3O_4@SiO_2 microspheres

The synthesis was carried out according to previous report with a little modification [22]. In a typical procedure, 20 mL ethanol and 4 mL deionized water were mixed together in a beaker, and then 0.2 g of prepared Fe_3O_4 microspheres was dispersed into the mixture by ultrasonication. Under constant mechanical stirring, 1 mL of ammonia solution (25%) and 0.8 mL of tetraethyl orthosilicate (TEOS) were consecutively added into the mixture. The mixture was further stirred for 3 h. The resultant products were collected and washed, and then dried under vacuum at 60 °C for 2 h for further use.

2.3. Synthesis of Fe_3O_4@SiO_2@MS microspheres

Fe_3O_4@SiO_2@PbS microspheres were synthesized as following: firstly, 0.04 g of Fe_3O_4@SiO_2 microspheres were dispersed into 60 mL of a 0.003 M lead dichloride solution, and the solution was stirred by a mechanical stirrer for 0.5 h to ensure sufficient adsorption of Pb^{2+} ions by the Fe_3O_4@SiO_2 microspheres. Then the microspheres were collected and washed twice with deionized water. Next, the microspheres were dispersed into 60 mL of a 0.1 M thioacetamide solution. The solution was heated with water bath at 45 °C for 1 h. During the heating process, the solution was also stirred by a mechanical stirrer. The final products were collected and washed, then dried under vacuum at 60 °C for 2 h. The whole synthesis procedure is shown in Scheme 1.

Fe_3O_4@SiO_2@ZnS and Fe_3O_4@SiO_2@HgS microspheres were synthesized similarly. Both the concentrations of Zn^{2+} and Hg^{2+} solutions used for the synthesis are 0.01 M.

2.4. Photocatalytic degradation of Rhodamin B

The photocatalytic degradation process was carried out as following: 40 mg of magnetic sulfide composites was dispersed into an aqueous solution of Rhodamin B (0.001 g/L, 50 mL). A 300 W column-like low-pressure mercury lamp was placed over the solution with a distance of 20 cm, and the solution was irradiated with the lamp under constant mechanical stirring and fan cooling. At intervals of 20 min, 3 mL of the solution was taken out and analyzed with a UV–vis absorption spectrometer.

2.5. Characterization

X-ray powder diffraction (XRD) patterns were obtained using a Shimadzu XRD-6000 X-ray diffractometer equipped with graphite monochromatized Cu Kα radiation (λ = 0.15406 nm). The field-emission scanning electron microscopy (FESEM) images were taken with a Hitachi S-4800 field-emission scanning electron microscope. Transmission electron microscopy (TEM) images and energy dispersive X-ray (EDX) spectrum were recorded on a JEOL-2010 high-resolution transmission electron microscope with energy dispersive X-ray analysis system. The magnetic hysteresis loops were recorded using a BHV-55 vibrating sample magnetometer (VSM) with an applied field between −5000 and 5000 Oe at room temperature. UV–vis absorption spectra were measured with a Shimadzu UV-3010 spectrometer.

3. Results and discussion

The as-obtained samples were examined by XRD. Fig. 1a shows a typical XRD pattern of the Fe_3O_4@SiO_2@PbS sample, in which all the diffraction peaks can be categorized into two sets. The diffraction peaks that labeled with "#" can be readily indexed to the orthorhombic phase of Fe_3O_4 (JCPDS card No. 75-1609), while the peaks marked with "$" can be indexed to the cubic phase of PbS (JCPDS card No. 05-0592). Several diffraction peaks of Fe_3O_4 and PbS are overlapped. No diffraction peaks corresponding to SiO_2 can be seen in the pattern mean that SiO_2 is amorphous. Fig. 1b and c shows typical XRD patterns of the Fe_3O_4@SiO_2@HgS and Fe_3O_4@SiO_2@ZnS composites. In addition to the diffraction peaks of Fe_3O_4, the diffraction peaks of HgS and ZnS are also observed. The weak diffraction peaks of ZnS indicate its poor crystallinity.

The morphology and size of the prepared samples were examined by FESEM. Fig. 2a shows a FESEM image of the Fe_3O_4 microspheres, in which many nearly monodisperse spherical particles with diameters of about 400 nm can be seen. The Fe_3O_4 microspheres are composed of many smaller nanoparticles, and their surfaces are rough. Fig. 2b is a FESEM image of the Fe_3O_4@SiO_2 microspheres. The smooth surfaces of the microspheres indicate the coating of SiO_2 layer on Fe_3O_4. The diameters of the Fe_3O_4@SiO_2 microspheres are not obviously enlarged, which reveals that the SiO_2 layer is thin. Fig. 2c and d shows FESEM images of the

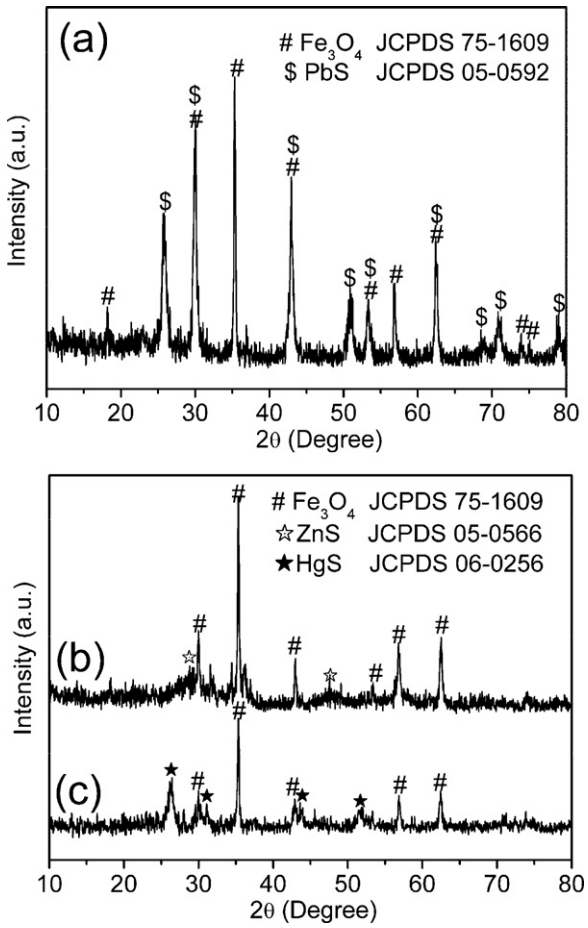

Fig. 1. XRD patterns of (a) Fe_3O_4@SiO_2@PbS microspheres, (b) Fe_3O_4@SiO_2@ZnS microspheres, and (c) Fe_3O_4@SiO_2@HgS microspheres.

Fe_3O_4@SiO_2@PbS microspheres with different magnifications. It can be clearly seen that many little PbS nanoparticles are adhered to the surfaces of the Fe_3O_4@SiO_2 microspheres. The PbS nanoparticles are uniform, with diameters of about 20 nm. Moreover, in this work, ZnS and HgS nanoparticles can also be deposited on the surfaces of Fe_3O_4@SiO_2 microspheres, as illuminated in Fig. 2e and f.

The morphology of the Fe_3O_4@SiO_2@PbS microspheres was further confirmed by TEM, as shown in Fig. 3a. The core–shell structure of the Fe_3O_4@SiO_2@PbS microspheres can be clearly seen. The diameter of Fe_3O_4 core is about 320 nm, the thickness of SiO_2 shell is about 30 nm, and the diameter of adhered PbS nanoparticles is about 20 nm. EDX spectrum of the Fe_3O_4@SiO_2@PbS microsphere is shown in Fig. 3b, in which Fe, O, Si, S, and Pb are all present. The EDX spectrum further confirms the composition of the Fe_3O_4@SiO_2@PbS microspheres.

The sulfide nanoparticles on the outside layer were formed due to the reaction between S^{2-} in the solution and metal ions adsorbed in SiO_2 layer. The amount of sulfide nanoparticles can be controlled by adjusting the amount of metal ions adsorbed in SiO_2 layer. Fig. 4a–d shows FESEM images of the Fe_3O_4@SiO_2@PbS microspheres obtained by dispersing Fe_3O_4@SiO_2 microspheres in 0.001 M, 0.002 M, 0.006 M, and 0.01 M Pb^{2+} solution for 0.5 h, respectively. From these figures we can learn that the amount of PbS nanoparticles on SiO_2 layer increases with increasing the concentration of Pb^{2+} solution. However, higher concentration of Pb^{2+} is not favorable for the uniformity of PbS nanoparticles. In Fig. 4d, besides PbS nanoparticles with the diameters of around 20 nm, the PbS nanoparticles with diameters of about 100 nm is

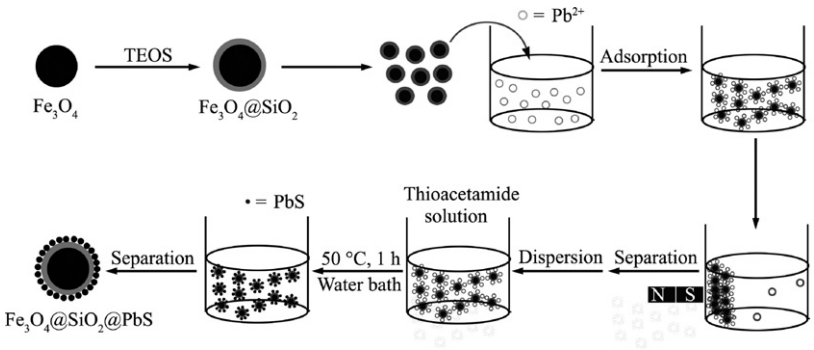

Scheme 1. Synthetic route of Fe_3O_4@SiO_2@PbS core–shell microspheres.

also observed. Because the adsorption ability of SiO_2 layer to Zn^{2+} and Hg^{2+} is not as strong as that to Pb^{2+} [18], the concentrations of Zn^{2+} and Hg^{2+} solutions used for the synthesis of Fe_3O_4@SiO_2@ZnS and Fe_3O_4@SiO_2@HgS is higher than that of Pb^{2+}.

Magnetic hysteresis loops of the Fe_3O_4 microspheres, Fe_3O_4@SiO_2 microspheres, and Fe_3O_4@SiO_2@PbS microspheres are shown in Fig. 5a. All of them show ferromagnetic behavior at room temperature. The magnetic saturation (*Ms*) values of the Fe_3O_4 microspheres, Fe_3O_4@SiO_2 microspheres, and Fe_3O_4@SiO_2@PbS microspheres are 80, 32, and 26 emu g^{-1}, respectively. The *Ms* values of Fe_3O_4@SiO_2 and Fe_3O_4@SiO_2@PbS microspheres are lower than that of the Fe_3O_4 microspheres due to low mass content of Fe_3O_4 in the Fe_3O_4@SiO_2 and Fe_3O_4@SiO_2@PbS microspheres. The Fe_3O_4@SiO_2@PbS microspheres with an excellent magnetic

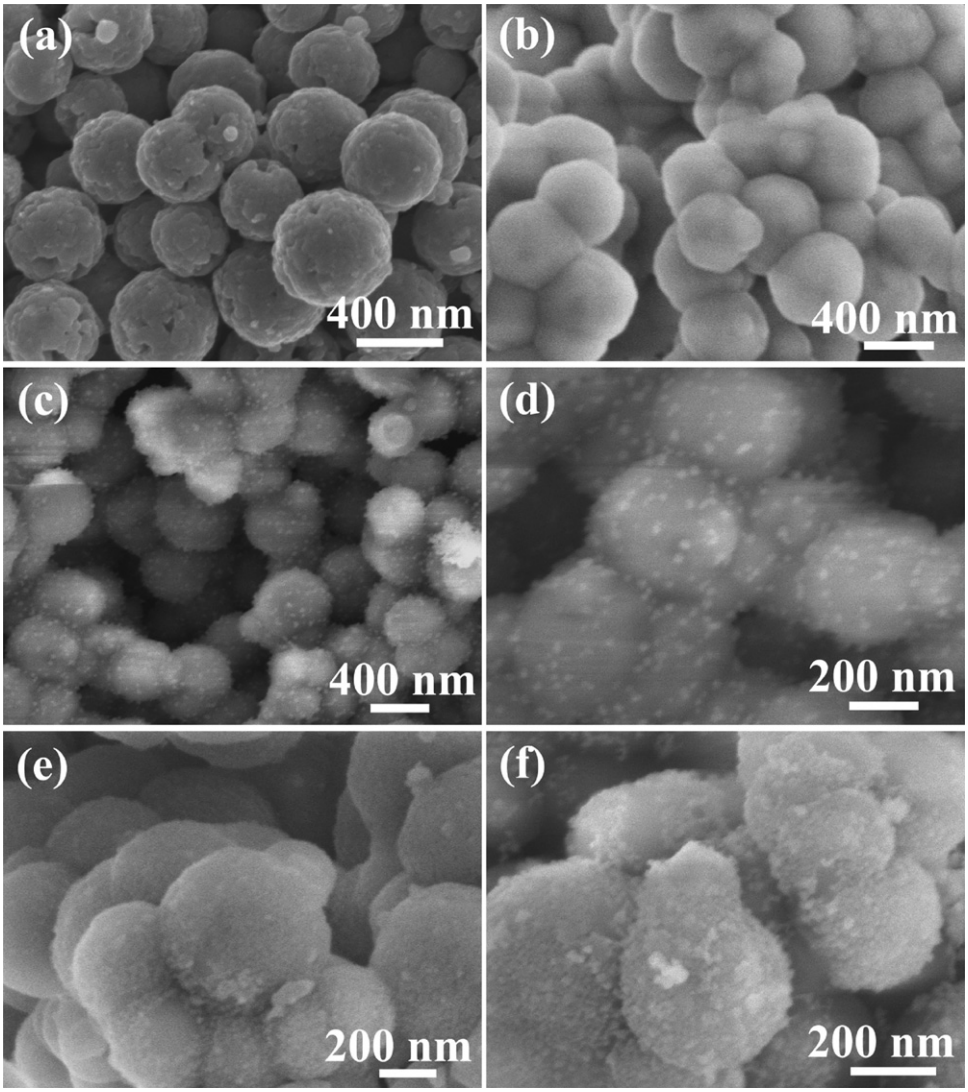

Fig. 2. FESEM images of (a) Fe_3O_4 microspheres, (b) Fe_3O_4@SiO_2 microspheres, (c and d) Fe_3O_4@SiO_2@PbS microspheres, (e) Fe_3O_4@SiO_2@ZnS microspheres, and (f) Fe_3O_4@SiO_2@HgS microspheres.

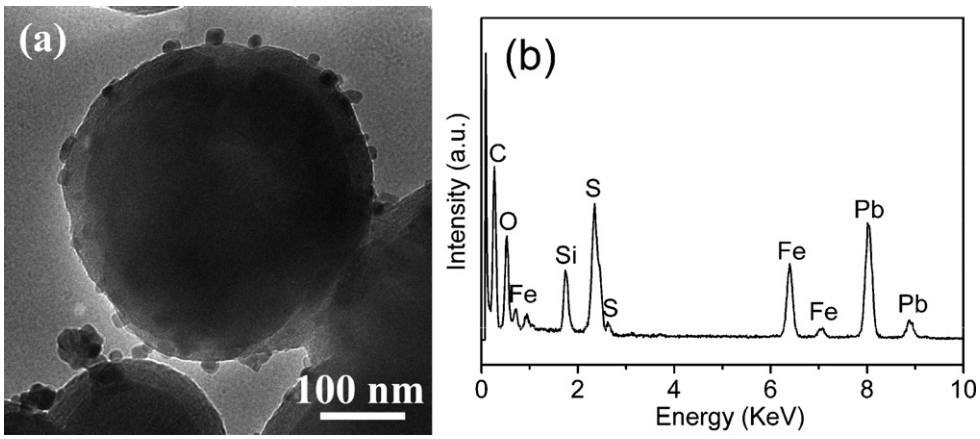

Fig. 3. (a) TEM image of the Fe_3O_4@SiO_2@PbS microspheres; (b) EDX spectrum of the Fe_3O_4@SiO_2@PbS microspheres.

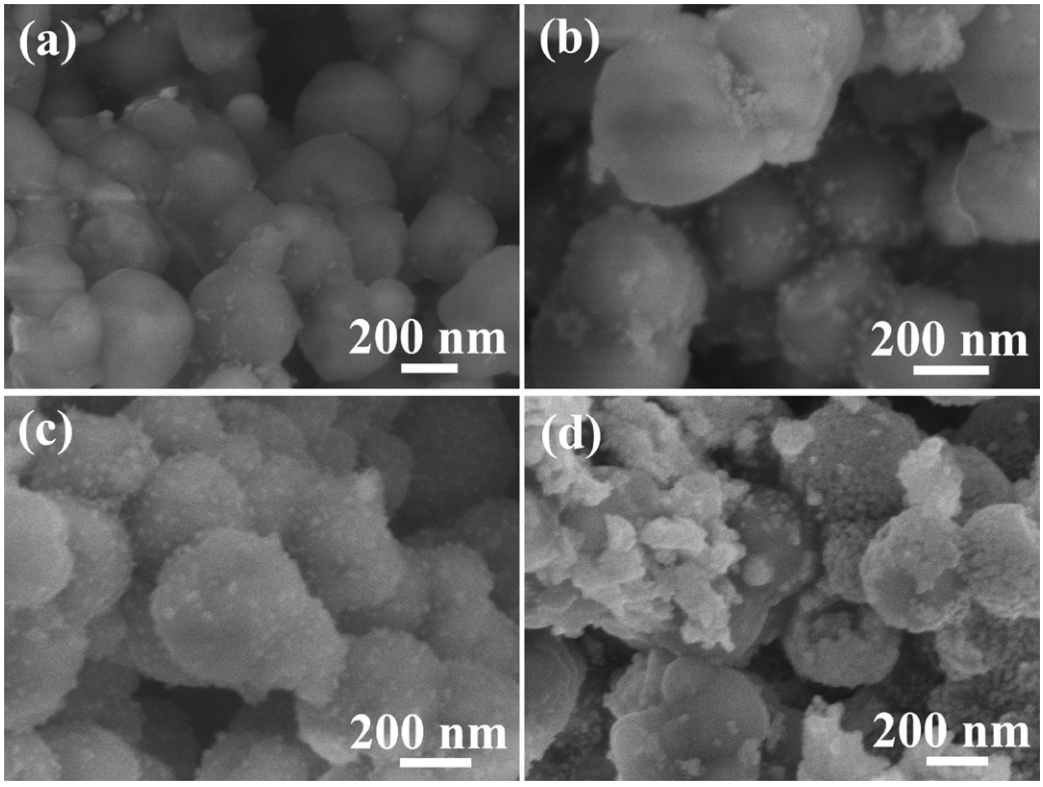

Fig. 4. FESEM images of the Fe_3O_4@SiO_2@PbS microspheres obtained with Pb^{2+} concentrations of (a) 0.001 M, (b) 0.002 M, (c) 0.005 M, and (d) 0.01 M.

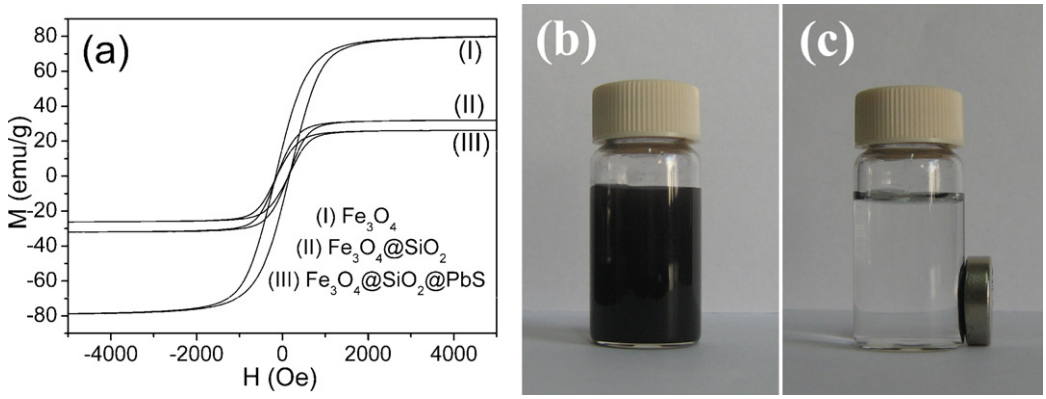

Fig. 5. (a) Hysteresis loops of Fe_3O_4 microspheres, Fe_3O_4@SiO_2 microspheres, and Fe_3O_4@SiO_2@PbS microspheres; (b) digital photograph of Fe_3O_4@SiO_2@PbS microspheres dispersed in water; (c) digital photograph of Fe_3O_4@SiO_2@PbS microspheres collected by an external magnet.

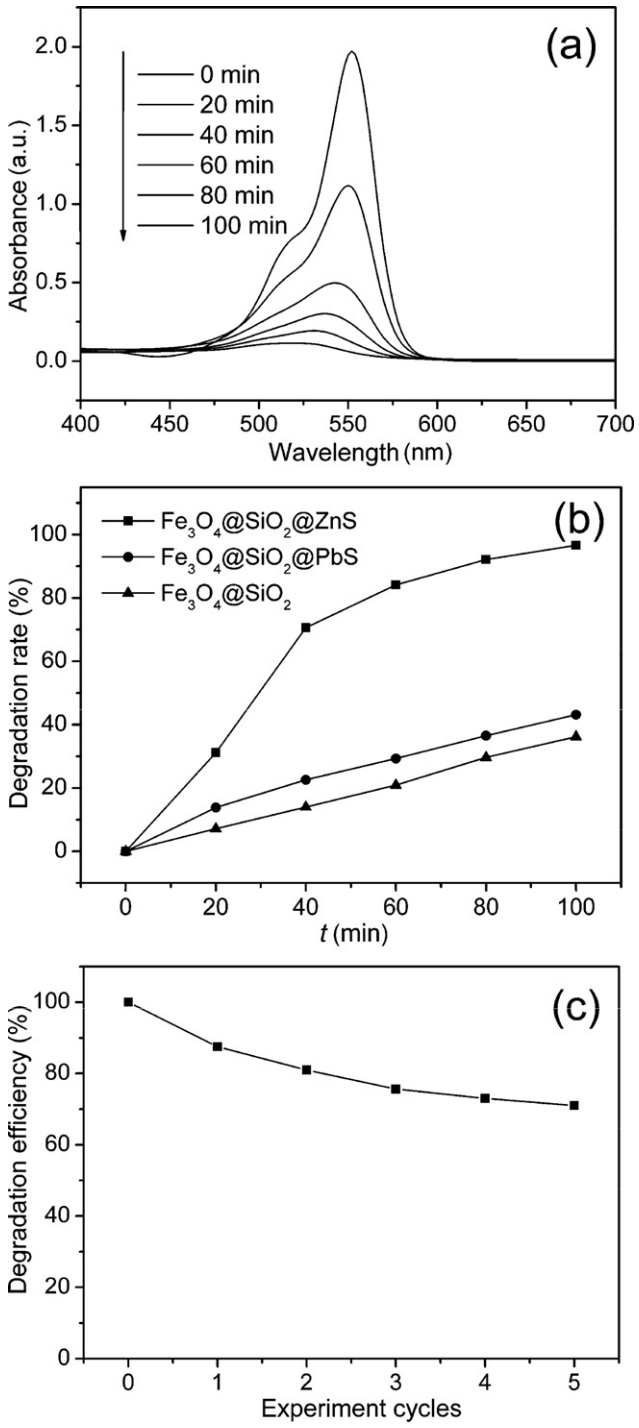

Fig. 6. (a) Time-dependent absorption spectra of a Rhodamin B aqueous solution (0.001 g/L, 50 mL) in the presence of Fe_3O_4@SiO_2@ZnS composites under exposure to UV light. (b) Degradation rate of Rhodamin B aqueous solution in the presence of Fe_3O_4@SiO_2@PbS, Fe_3O_4@SiO_2@ZnS, and Fe_3O_4@SiO_2 composites, respectively. (c) Relationship between the degradation efficiency of Fe_3O_4@SiO_2@ZnS photocatalyst and cyclic time.

property are easily separated from solution with the help of an external magnetic force. Fig. 5b shows a digital photograph of the Fe_3O_4@SiO_2@PbS microspheres that dispersed in water. After a magnet was placed aside, the black microspheres can be magnetized in several seconds, leaving a clear solution (Fig. 5c).

Semiconductor-type photocatalysts have been widely used for the photodegradation of water pollutants such as dyes and halogenated benzene derivatives [23–25]. Here the prepared magnetic sulfide composites have a layer of semiconductor nanoparticles on their surfaces, and the sizes of the semiconductor nanoparticles are very small, which result in the high surface-to-volume ratio. So the magnetic sulfide nanocomposites may exhibit excellent photocatalytic activities. Furthermore, the photodegradation of water pollutants is occurred in water, and an additional separation step to remove the catalysts from the treated water is necessary. The common ways to remove the catalysts are filtration and centrifugation, which are fuzzy and slow, and may drawback to the application of the photocatalytic process for treating wastewaters. The prepared magnetic sulfide composites have magnet core, which enables them be conveniently and quickly removed from water via an external magnet. Thus, it is reasonable to expect the as-prepared magnetic sulfide composites be used as ideal recyclable photocatalysts in practical applications.

The photocatalytic activities of the magnetic sulfide composites were evaluated by photodegradation of Rhodamin B under the illumination of UV light. Fig. 6a shows the time-dependent UV–vis absorption spectra of Rhodamin B aqueous solution in the presence of Fe_3O_4@SiO_2@ZnS microspheres under the illumination of UV light. The intensity of absorption peaks centered at 550 nm gradually decrease with increasing time due to the concentration decreasing of Rhodamin B. This result indicates that Rhodamin B is gradually degraded under UV light irradiation with the presence of Fe_3O_4@SiO_2@ZnS microspheres. Fig. 6b shows the degradation rate of Rhodamin B solution irradiated under UV light with the same mass of Fe_3O_4@SiO_2@ZnS, Fe_3O_4@SiO_2@PbS, and Fe_3O_4@SiO_2 composites, respectively. The Fe_3O_4@SiO_2@PbS composites were prepared with Pb^{2+} concentration of 0.01 M. After 100 min UV irradiation, the degradation rates of Rhodamin B reach 96%, 43%, and 36%. This result shows that although Fe_3O_4@SiO_2 composites alone can degrade Rhodamin B under the illumination of UV light, the coating of sulfide nanoparticles on the surfaces of Fe_3O_4@SiO_2 composites can obviously promote the degradation rates of Rhodamin B. The degradation efficiency of Fe_3O_4@SiO_2@ZnS composites is much better than that of Fe_3O_4@SiO_2@PbS, because ZnS has much better photocatalytic efficiency than PbS.

The photocatalytic efficiency of the Fe_3O_4@SiO_2@ZnS microspheres for recyclable usage was studied. Fig. 6c shows the photocatalytic efficiency of the Fe_3O_4@SiO_2@ZnS composites after 5 cycles. The result shows that the photocatalytic activity of the Fe_3O_4@SiO_2@ZnS composites only decreased a little after 5 cycles of the photocatalysis experiments. The reason may be that some of the ZnS nanoparticles are broken away from the Fe_3O_4@SiO_2@ZnS composites when they are stirred, as a result, the photocatalytic efficiency of the Fe_3O_4@SiO_2@ZnS composites decrease.

4. Conclusions

In summary, Fe_3O_4@SiO_2@MS (M = Pb, Zn, and Hg) microspheres with well-defined core–shell structures were successfully prepared by using a facile wet chemical method. The multi-layered composites have the merit of multi-functional and stability. Photocatalytic experiments show that the prepared Fe_3O_4@SiO_2@ZnS microspheres have good photocatalytic activities under the illumination of UV light, and can be applied as recyclable photocatalysts.

Acknowledgement

Financial supports from the National Natural Science Foundation of China (20701001) and Anhui Key Laboratory of Controllable Chemistry Reaction & Material Chemical Engineering are gratefully acknowledged.

References

[1] F. Caruso, Adv. Mater. 13 (2001) 11–22.
[2] K.J.C. Van Bommel, A. Friggeri, S. Shinkai, Angew. Chem. Int. Ed. 42 (2003) 980–999.
[3] X.W. Teng, D. Black, N.J. Watkins, Y.L. Gao, H. Yang, Nano Letters 3 (2003) 261–264.
[4] J.Y. Li, S.L. Xiong, J. Pan, Y.T. Qian, J. Phys. Chem. C 114 (2010) 9645–9650.
[5] C.L. Zhu, M.L. Zhang, Y.J. Qiao, G. Xiao, F. Zhang, Y.J. Chen, J. Phys. Chem. C 114 (2010) 16229–16235.
[6] J.Q. Hu, Y. Bando, J.H. Zhan, D. Golberg, Appl. Phys. Lett. 85 (2004) 3593–3595.
[7] B. Liu, H.C. Zeng, Small 1 (2005) 566–571.
[8] J. Cao, J.Z. Sun, J. Hong, H.Y. Li, H.Z. Chen, M. Wang, Adv. Mater. 16 (2004) 84–87.
[9] X.M. Sun, Y.D. Li, Angew. Chem. Int. Ed. 43 (2004) 597–601.
[10] Q.B. Wang, Y. Liu, Y.G. Ke, H. Yan, Angew. Chem. Int. Ed. 47 (2008) 316–319.
[11] J.L. Lyon, D.A. Fleming, M.B. Stone, P. Schiffer, M.E. Williams, Nano Letters 4 (2004) 719–723.
[12] P.P. Yang, Z.W. Quan, Z.Y. Hou, C.X. Li, X.J. Kang, Z.Y. Cheng, J. Lin, Biomaterials 30 (2009) 4786–4795.
[13] M. Zhang, Y.P. Wu, X.Z. Feng, X.W. He, L.X. Chen, Y.K. Zhang, J. Mater. Chem. 20 (2010) 5835–5842.
[14] S.S. Liu, H.M. Chen, X.H. Lu, C.H. Deng, X.M. Zhang, P.Y. Yang, Angew. Chem. Int. Ed. 49 (2010) 7557–7561.
[15] Y.H. Won, D. Aboagye, H.S. Jang, A. Jitianu, L.A. Stanciu, J. Mater. Chem. 20 (2010) 5030–5034.
[16] Y. Li, J.S. Wu, D.W. Qi, X.Q. Xu, C.H. Deng, P.Y. Yang, X.M. Zhuang, Chem. Commun. (2008) 564–566.
[17] X.W. Liu, Q.Y. Hu, Z. Fang, X.J. Zhang, B.B. Zhang, Langmuir 25 (2009) 3–8.
[18] H.B. Hu, Z.H. Wang, L. Pan, J. Alloy Compd. 492 (2010) 656–661.
[19] Y. Li, X.Q. Xu, D.W. Qi, C.H. Deng, P.Y. Yang, X.M. Zhang, J. Proteome Res. 7 (2008) 2526–2538.
[20] H.B. Hu, Z.H. Wang, L. Pan, S.P. Zhao, S.Y. Zhu, J. Phys. Chem. C 114 (2010) 7738–7742.
[21] H. Deng, X.L. Li, Q. Peng, X. Wang, J.P. Chen, Y.D. Li, Angew. Chem. Int. Ed. 44 (2005) 2782–2785.
[22] W. Stöber, A. Fink, E. Bohn, J. Colloid Interface Sci. 26 (1968) 62–69.
[23] Y.C. Chen, C.H. Wang, H.Y. Lin, B.H. Li, W.T. Chen, C.P. Liu, Nanotechnology 21 (2010) 455604.
[24] D.G. Chen, F. Huang, G.Q. Ren, D.S. Li, M. Zheng, Y.J. Wang, Z. Lin, Nanoscale 2 (2010) 2062–2064.
[25] H.B. Yin, Y. Wada, T. Kitamura, S. Yanagida, Environ. Sci. Technol. 35 (2001) 227–231.